ELSEVIER

Journal of Non-Crystalline Solids 266–269 (2000) 765–768

JOURNAL OF NON-CRYSTALLINE SOLIDS

www.elsevier.com/locate/jnoncrysol

Determination of bonding in amorphous carbons by electron energy loss spectroscopy, Raman scattering and X-ray reflectivity

A.C. Ferrari [a], B. Kleinsorge [a], G. Adamopoulos [a], J. Robertson [a,*], W.I. Milne [a], V. Stolojan [b], L.M. Brown [b], A. LiBassi [c], B.K. Tanner [c]

[a] *Department of Engineering, Cambridge University, Trumpington Street, Cambridge CB2 1PZ, UK*
[b] *Cavendish Labs, Cambridge University, Cambridge CB3 0HE, UK*
[c] *Department of Physics, Durham University, Durham, UK*

Abstract

X-ray reflectivity (XRR) and Raman scattering are developed as non-destructive methods to find the density and sp^3 content of unhydrogenated and hydrogenated amorphous carbon films. An empirical relationship is found to derive the sp^3 fraction from visible Raman spectra, while ultraviolet (UV) Raman is able to directly detect sp^3 sites. The sp^3 fraction and density are linearly correlated in amorphous carbon (a-C) and hydrogenated amorphous carbon (a-C:H) films.

The properties of diamond-like carbons (DLCs) depend primarily on the fraction of sp^3 and sp^2 sites, the hydrogen content and the ordering of sp^2 sites [1]. At present electron energy loss spectroscopy (EELS) is the preferred method to determine sp^3 fraction, because this method not only gives the sp^2 content from the relative size of the π^* peak on the carbon K edge, but also the valence plasmon at 26–34 eV gives the mass density, which is often proportional to the sp^3 fraction [2]. However, EELS is a destructive and time-consuming method, so other non-destructive methods would be valuable. This paper describes advances in the use of two widely available, non-destructive methods, glancing angle X-ray reflectivity (XRR) to give the film density [3], and secondly Raman and ultraviolet (UV) Raman scattering to provide information on sp^3 content.

The refractive index of materials to X-rays is just under 1, so that X-rays are totally internally reflected within the air when incident at a grazing angle. The critical angle θ_c for total internal reflection is given by [3]

$$\theta_c = \lambda\left(\frac{N_A r_0 \rho}{\pi}\frac{[X_C Z_C + X_H Z_H]}{X_C M_C + X_H M_H}\right)^{1/2}, \quad (1)$$

where λ is the X-ray wavelength, $r_0 = e^2/4\pi\epsilon_0 mc^2$ the classical electron radius, M_C the molar mass of carbon, N_A the Avogadro's number, Z_i are the atomic numbers, X_i the atomic fractions, and ρ is the mass density. Writing $X_C = 1 - X_H$, the mass density ρ becomes

$$\rho = \frac{\pi^2 c^2 \epsilon_0}{3\lambda^2 N_A e^2} M_C M_e \theta_c^2 \frac{12 - 11X_H}{6 - 5X_H}. \quad (2)$$

* Corresponding author. Tel.: +44-1223 33 2689; fax: +44-1223 33 2662.
E-mail address: jr@eng.cam.ac.uk (J. Robertson).

0022-3093/00/$ - see front matter
PII: S0022-3093(00)00035-1

Fig. 1 shows the reflected intensity from a tetrahedral amorphous carbon (ta-C) film on a silicon substrate. The reflected intensity drops sharply above θ_c, and shows a series of oscillations as it declines. For high density carbon films such as ta-C, the main critical angle is due to the *C* film. However, lower density films on Si such as a-C:H have an electron density less than Si, so the main θ_c is from the a-C:H/Si interface, and the a-C:H/air interface gives a subsiduary critical angle at a smaller angle. The intensity oscillations beyond θ_c due to the interference between beams reflected from the surface and substrate/film interface give the film thickness. The longer period oscillation is due to internal layering. The complete information on density, film thickness, surface roughness and the presence of internal layering is obtained by modelling the reflections from the film/substrate pair. In this way, XRR can give the density and thickness of carbon films to high precision (0.05 g/cm^3 and 0.1 nm) [4].

The mass density was previously derived from valence plasmon energy, E_p, measured by EELS using $E_p = \hbar(ne^2/\varepsilon_0 m^*)^{1/2}$ or

$$\rho = \left(\frac{\varepsilon_0 M_C m^* E_p^2}{12\hbar^2 N_A e^2}\right)\frac{12 - 11X_H}{4 - 3X_H}, \quad (3)$$

where n is the valence electron density, m^* the electron effective mass, ε_0 the permittivity of free space and E_p is in eV. Comparing the derivation of density from XRR and plasmon energies, Eqs. (2) and (3), the X-ray critical angle is proportional to the total number of electrons, whereas the plasmon energy is proportional to the valence electrons. Thus, XRR density is less sensitive to *H* content than the plasmon energy, which is an advantage as *H* content is often less well known.

Eq. (3) assumes that valence electrons behave like free electrons. This approximation works, but it is necessary to use an electron effective mass m^* of 0.85 to give the observed plasmon energy of diamond (33.8 eV). It is unclear if the same m^* holds for all carbons. Taking the mass densities of various carbon films found by XRR and plasmon energies, we find that $m^* = 0.87$ gives a common fit to all plasmon energies, so this approximation holds [4].

Fig. 2 shows the density derived by XRR and from plasmon energies with this m^* value plotted against sp^3 fraction for ta-C deposited by a filtered cathodic vacuum arc (FCVA) and ta-C:H deposited by plasma beam source (PBS) or by an electron cyclotron wave resonance (ECWR) system.

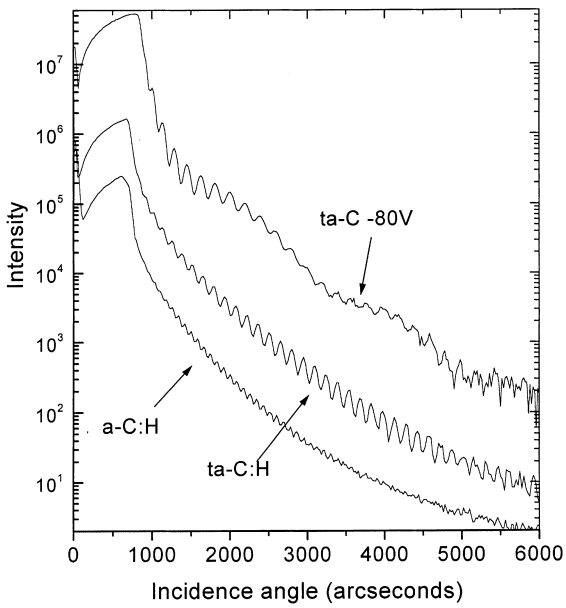

Fig. 1. X-ray reflectivity vs scattering angle, for ta-C, ta-C:H and a-C:H films on Si substrates.

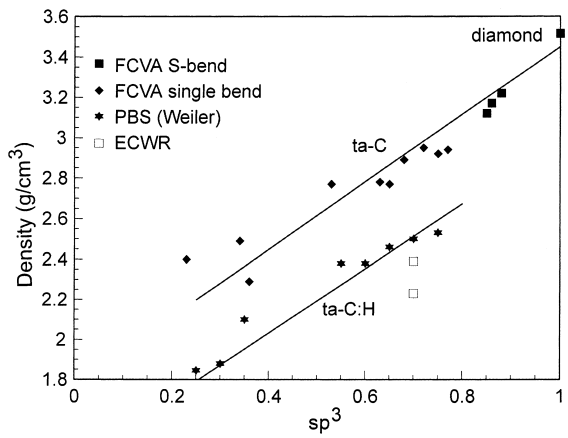

Fig. 2. Variation of density with sp^3 fraction for ta-C films grown by FCVA and ta-C:H films grown by PBS and ECWR. Lines are guide to eye.

The density and sp^3 content varies roughly linearly for the two types of DLCs. The highest density for ta-C is 3.26 ± 0.05 g/cm^3 for 88% sp^3 fraction, whereas the ta-C:H has a lower density of 2.36 g/cm^3 for 70% sp^3 fraction.

The sp^3 fraction is found from the carbon K edge EELS spectrum. The sp^2 fraction is derived by taking the ratio of areas of the 285 eV peak due to π states and 290 eV edge due to σ states, and comparing this to their ratio in graphite which is 100% sp^2 [2].

Raman scattering using visible photons is a popular method to probe the quality of CVD diamond and DLC. However, the visible Raman spectra of DLCs is dominated by the sp^2 sites, which have a ~55 times larger cross-section than sp^3 sites, because visible photons are only able to excite π states. The Raman spectra of carbons is dominated by two features, a G peak at around 1550 cm^{-1} and a D mode around 1350 cm^{-1} [5]. The G peak is derived from the zone centre E_{2g} bond stretching mode of graphite, and is present in all sp^2 bonded carbons. The D mode is a disorder-activated K zone boundary mode, due to the A_{1g} symmetry breathing motion of 6-fold aromatic rings, which requires the presence of such rings. The interesting feature of Raman in disordered carbon is that the Raman spectra are dominated by these two features, rather than resembling the phonon density of states as it does in a-Si [6].

A detailed analysis of the variation of the Raman spectra of carbon on their bonding finds that the spectra depend fundamentally on the ordering of the sp^2 sites [7]: whether sp^2 sites form rings or chains, the density of aromatic rings, and the size of the aromatic ring clusters. If the sp^3 and sp^2 phases in DLCs are related, for example by the deposition process, so that the ordering of the sp^2 phase evolves as the sp^3 fraction increases, then we may use Raman spectra to derive sp^3 content empirically.

Fig. 3(a) shows the G peak wavenumber (measured at 514 nm) plotted against (Tauc) optical gap for plasma deposited a-C:H from data of Tamor and Vassell [8]. We previously found that the optical gap of a-C:H varies systematically with sp^3 content derived from EELS or NMR [9] (Fig. 4). This variation allows us to plot G wavenumber

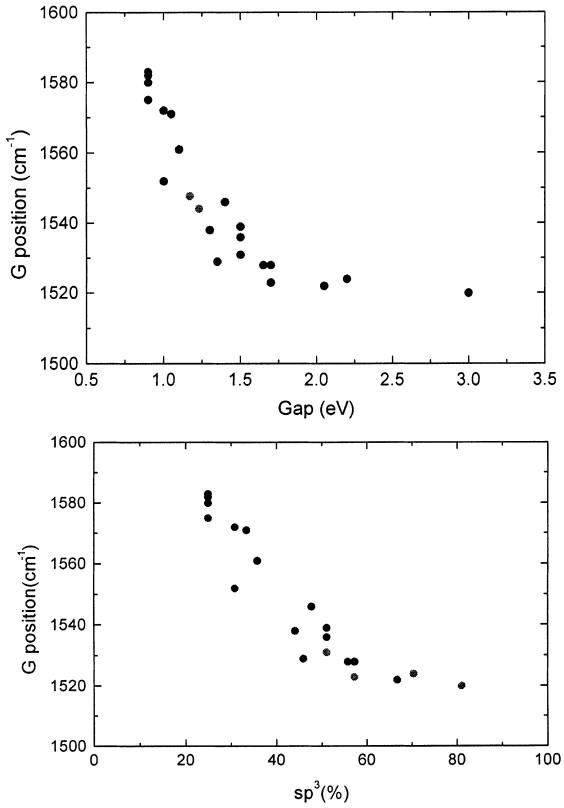

Fig. 3. G peak wavenumber vs: (a) optical (Tauc) gap and (b) sp^3 fraction, for as-deposited a-C:H films (data from Tamor and Vassell [8]) for excitation at 514 nm.

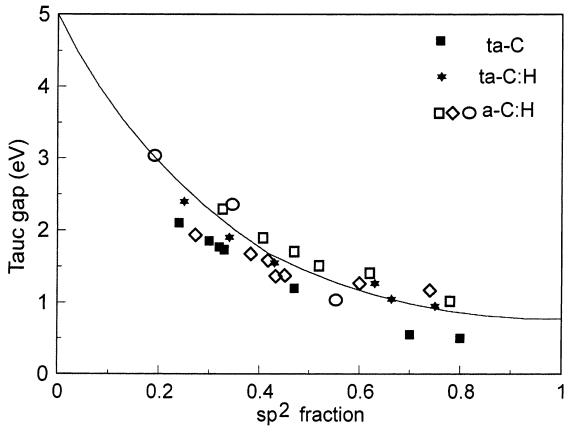

Fig. 4. Tauc gap vs sp^2 content for various a-C and a-C:H films [9]. Lines are guide to eye.

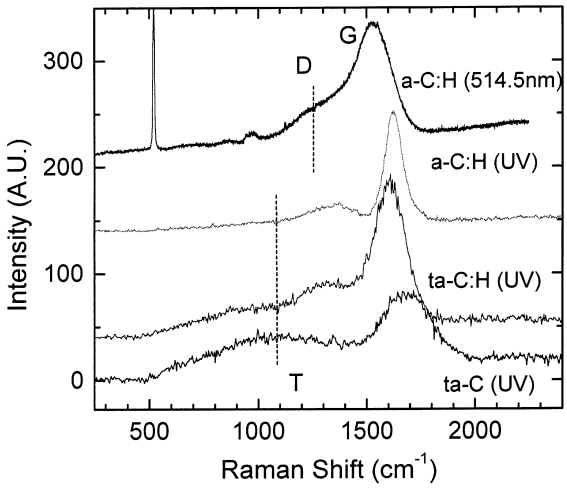

Fig. 5. UV (244 nm) Raman spectra of ta-C, ta-C:H and a-C:H and a visible Raman spectrum of a-C:H.

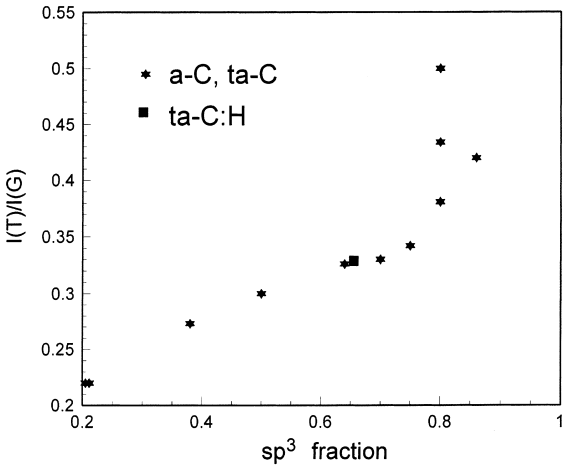

Fig. 6. Variation of UV Raman T to G peak area vs sp^3 fraction for various carbon films.

against sp^3 content (Fig. 3(b)). It is seen that the G peak decreases almost linearly with increasing sp^3 content, and may saturate at the highest sp^3 content. As the sp^3 content increases in a-C:H, the sp^2 site ordering changes from aromatic clusters at large sp^2 content, through single aromatic rings and olefinic chains in diamond-like a-C:H, to shorter olefinic chains in polymeric a-C:H, and this process causes the G peak to shift downwards.

The sp^3 sites are not directly observed in visible Raman. The higher photon energies of UV Raman can excite the σ states of sp^3 sites. The UV Raman spectra of ta-C shows a new broad peak at 1100 cm^{-1} labeled as T peak, attributed to sp^3 sites [10] (Fig. 5) The G peak is still present in UV Raman, and has now moved to a higher wavenumber. It is found that the ratio of areas of T to G peak correlates well with the sp^3 content for ta-C [11]. The UV Raman spectra of other DLCs such as ta-C:H and a-C:H have been measured (Fig. 6). There is now a much broader feature below the G peak instead of a single T peak. There are a number of contributions to this feature, including C–H bending modes, which need to be further studied. Thus, the ratio of T to G peak areas is a rough guide to the sp^3 content [12], but further work is needed to provide a reliable relationship.

References

[1] J. Robertson, Prog. Solid State Chem. 21 (1991) 199.
[2] P.J. Fallon, V.S. Veerasamy, C.A. Davis, J. Robertson, G.A.J. Amaratunga, W.I. Milne, J. Koskinen, Phys. Rev. B 48 (1993) 4777.
[3] F. Toney, S. Brennan, J. Appl. Phys. 66 (1989) 1861.
[4] A. Li Bassi, A.C. Ferrari, V. Stolojan, B.K. Tanner, J. Robertson, L.M. Brown, Diamond Related Mater. (2000) in press.
[5] R.J. Nemanich, S.A. Solin, Phys. Rev. B 20 (1979) 392.
[6] R. Alben, D. Weaire, J.E. Smith, M.H. Brodsky, Phys. Rev. B 11 (1975) 2271.
[7] A.C. Ferrari, J. Robertson, Mater. Res. Soc. Symp. Proc. 593 (1999).
[8] M.A. Tamor, W.C. Vassell, J. Appl. Phys. 76 (1994) 3823.
[9] J. Robertson, Phys. Rev. B 53 (1996) 16302.
[10] K.W.R. Gilkes, H.S. Sands, D.N. Batchelder, J. Robertson, W.I. Milne, Appl. Phys. Lett. 70 (1997) 1980.
[11] S. Prawer, K.W. Nugent, in: S.R.P. Silva et al. (Eds.), Amorphous Carbon State of Art, World Scientific, Singapore, 1998.
[12] G. Adamopoulos, K.W.R. Gilkes, J. Robertson, N.M.J. Conway, B.Y. Kleinsorge, A. Buckley, D.N. Batchelder, Diamond Related Mater. 8 (1999) 541.